Geochemistry Geophysics Geosystems G3
AN ELECTRONIC JOURNAL OF THE EARTH SCIENCES
Published by AGU and the Geochemical Society

Article
Volume 4, Number 2
22 February 2003
1020, doi:10.1029/2001GC000207
ISSN: 1525-2027

Constraint of fault parameters inferred from nonplanar fault modeling

Hideo Aochi and Raul Madariaga
Laboratoire de Géologie, École Normale Supérieure, 24 rue Lhomond, 75231 Paris Cedex 05, France (aochi@geologie.ens.fr; madariag@geologie.ens.fr)

Eiichi Fukuyama
National Research Institute for Earth Science and Disaster Prevention, 3-1 Tennodai, Tsukuba 305-0006, Japan (fuku@bosai.go.jp)

[1] We study the distribution of initial stress and frictional parameters for the 28 June 1992 Landers, California, earthquake through dynamic rupture simulation along a nonplanar fault system. We find that observational evidence of large slip distribution near the ground surface requires large nonzero cohesive forces in the depth-dependent friction law. This is the only way that stress can accumulate and be released at shallow depths. We then study the variation of frictional parameters along the strike of the fault. For this purpose we mapped into our segmented fault model the initial stress heterogeneity inverted by *Peyrat et al.* [2001] using a planar fault model. Simulations with this initial stress field improved the overall fit of the rupture process to that inferred from kinematic inversions, and also improved the fit to the ground motion observed in Southern California. In order to obtain this fit, we had to introduce an additional variations of frictional parameters along the fault. The most important is a weak Kickapoo fault and a strong Johnson Valley fault.

Components: 6946 words, 11 figures, 4 videos.

Keywords: Landers earthquake; Boundary integral equation method; Fault geometry; Rupture dynamics; Ground motion.

Index Terms: 7209 Seismology: Earthquake dynamics and mechanics; 7212 Seismology: Earthquake ground motions and engineering; 8123 Tectonophysics: Dynamics, seismotectonics; 8164 Tectonophysics: Evolution of the Earth: Stresses—crust and lithosphere.

Received 27 July 2001; **Revised** 30 July 2002; **Accepted** 17 October 2002; **Published** 22 February 2003.

Aochi, H., R. Madariaga, and E. Fukuyama, Constraint of fault parameters inferred from nonplanar fault modeling, *Geochem. Geophys. Geosyst.*, *4*(2), 1020, doi:10.1029/2001GC000207, 2003.

1. Introduction

[2] Since the studies of *Harris et al.* [1991] and *Harris and Day* [1993], dynamic rupture propagation along nonplanar faults has been simulated using the finite difference method (FDM) [*Kase and Kuge*, 1998, 2001; *Harris and Day*, 1999]. Unfortunately, 3-D finite difference can not model fault branching, fault curvature and other geometrical complexities without major changes in its current formulation. Thanks to rapid progress in the development of boundary integral equation methods (BIEM), originally proposed by *Koller et al.* [1992], *Cochard and Madariaga* [1994] and *Fukuyama and Madariaga* [1995], it is now possible to model complex fault systems consisting of

several subfaults, including branched and bent faults [*Kame and Yamashita*, 1997; *Tada and Yamashita*, 1997; *Aochi et al.*, 2000a]. These methods can also be applied to study spontaneous crack propagation in intact material [*Kame and Yamashita*, 1999]. Based on these recent studies, *Aochi and Fukuyama* [2002] modeled the 1992 Landers earthquake, using a realistic nonplanar fault geometry learned from field observations, a loading system (remote tectonic stress) derived from geological considerations, and a depth-dependent slip-weakening law. In this paper, we investigate the initial condition of the friction law for the simulation of the Landers earthquake.

[3] For the purpose of understanding earthquakes, we have to study the role of the friction law that controls rupture process. Since rupture process are very complex and spatially heterogeneous, frictional parameters or stress field are probably also very heterogeneous. We know from fracture physics that spontaneous rupture propagation requires stress release in order to propagate, so that we need an opposite mechanism in order to stop the rupture process. The effect of frictional parameters are well understood in numerical experiments [*Boatwright and Cocco*, 1996]. On the other hand, it is very difficult to determine them quantitatively for a real earthquake in the field. For the Landers earthquake, the stress change during the earthquake was very heterogeneous along the fault as determined from kinematic fault models [*Wald and Heaton*, 1994; *Bouchon et al.*, 1998a; *Day et al.*, 1998] and dynamic modeling and inversion [*Olsen et al.*, 1997; *Peyrat et al.*, 2001]. The relation between shear stress and fault movement was also determined from kinematic inversions of the 1995 Hyogoken-nanbu, Japan, earthquake [*Ide and Takeo*, 1997; *Guatteri and Spudich*, 2000; *Guatteri et al.*, 2001]. But according to these authors, the resolution of these estimations is limited because of the finite frequency band used in the kinematic inversion. Usual kinematic inversions can only determine relative dynamic stress changes during rupture. In recent works, there have been attempts to investigate the absolute level of stress field [*Bouchon et al.*, 1998b; *Spudich et al.*, 1998]. One of the results that appears from these works is that the accumulated stress is much less than the stress extrapolated from laboratory experiments.

[4] In spite of the difficulty and uncertainty of the estimation of fault parameters, we absolutely need them for reproducing the rupture branching phenomena in numerical simulations. In this paper, we focus on the question of how to constrain them from observations of rupture of the Landers earthquake. As shown by *Aochi et al.* [2000a, 2000b], the absolute level of stress and frictional parameters appear explicitly in nonplanar fault systems, because the external tectonic forces produces heterogeneous stress distribution depending on fault orientation (strike). In a recent simulation, *Aochi and Fukuyama* [2002] succeeded in reproducing the general rupture propagation of the Landers earthquake without any horizontal heterogeneity of fault parameters. Rupture complexity was only due to a heterogeneous stress field produced by the assumed tectonic loading forces. In the previous model [*Aochi and Fukuyama*, 2002], an external loading force, whose direction changed regionally according to local tectonics, produced heterogeneity not in fault parameters but in initial stress field along the fault system. That model successfully reproduced realistic rupture transfer between faults. For instance, rupture progressed not along the northern Johnson Valley fault, but propagated into the Kickapoo and the Homestead Valley faults, as shown in the map of Figure 1.

[5] In this paper we will test several rupture scenarios for the Landers earthquake. In a first step we consider the variation of the friction law with depth. As proposed by *Scholz* [1988], cohesive force is usually assumed to be zero at the ground surface in some seismic rupture simulations [*Yamashita and Ohnaka*, 1992]; whereas other simulations did not assume any depth-dependency [*Olsen et al.*, 1997; *Peyrat et al.*, 2001]. Here we will discuss the question of how cohesive force may affect rupture propagation and strong ground motion. In the second part, we will discuss the horizontal heterogeneity of frictional parameters. We first assume a uniform external load (remote tectonic stress). We will investigate what kind of heterogeneity of fault parameters is required so that rupture chooses the

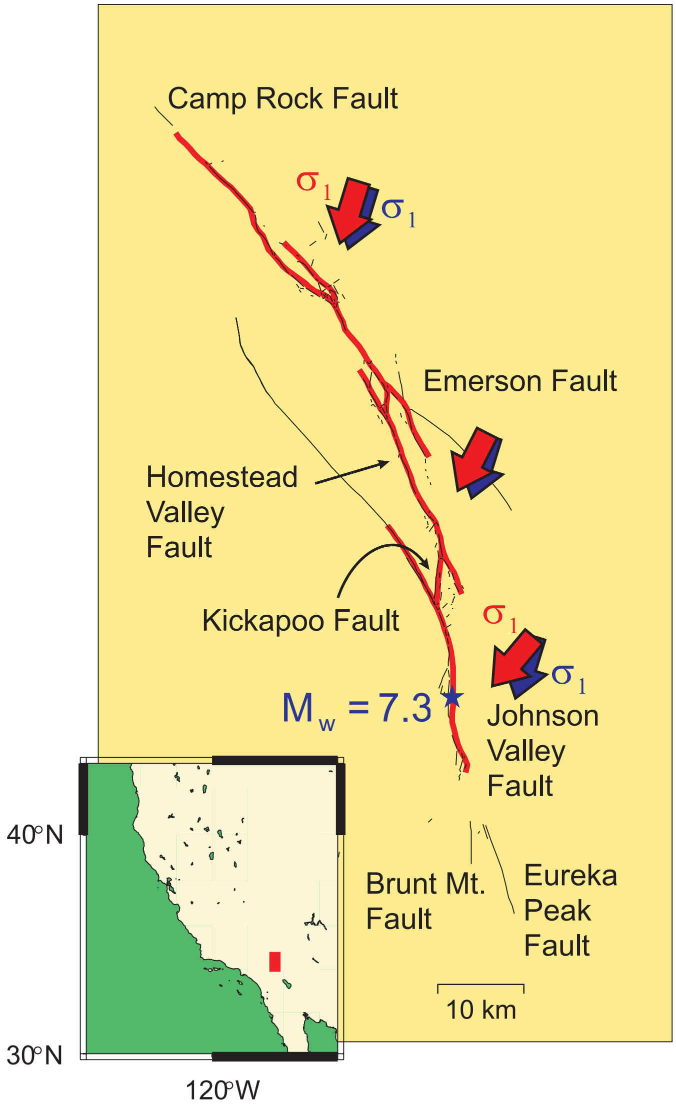

Figure 1. Fault model (red lines) studied by *Aochi and Fukuyama* [2002]. Black lines are the trace of observed active faults [*Hart et al.*, 1993]. Arrows represent the assumed directions of the maximum principal stress σ_1 (red, spatially rotating principal stress assumed by *Aochi and Fukuyama* [2002]; blue, uniform stress field used in this study).

correct fault branches, and we will compare with the previous heterogeneous external load case [*Aochi and Fukuyama*, 2002]. We finally study the mapping of the heterogeneity of initial stress obtained from a planar fault inversion [*Peyrat et al.*, 2001] onto our segmented fault model, and compare rupture propagation and seismic radiation.

2. The Nonplanar Fault Model of *Aochi and Fukuyama* [2002]

[6] For planar fault simulations, one needs to specify the initial shear stress on the fault and its constitutive parameters [e.g., *Olsen et al.*, 1997]. For nonplanar fault modeling, on the other hand, we need absolute stress values [*Aochi et al.*, 2000a]. *Aochi and Fukuyama* [2002] constructed a nonplanar fault model based on the surface fault traces [*Hart et al.*, 1993] shown in Figure 1. It is important to remark that the model included both the faults that did break during the 1992 rupture and those that did not; so that the model allowed the rupture to progress along any fault segment. The fault segments that the rupture chose depended on the initial stress field and fault properties.

[7] For the initial stress field, *Aochi and Fukuyama* [2002] assumed an external load (remote tectonic stress) based on geological studies of local tectonics [*Dokka and Travis*, 1990; *Unruh et al.*, 1994; *Sowers et al.*, 1994]. The red arrows in Figure 1 shows the maximum principal stress σ_1 assumed in their simulation. The direction of σ_1 points in the NNE direction except in the southern part of the rupture area (Johnson Valley, Kickapoo, and southern Homestead Valley faults) where it is closer to the NE direction. The depth dependence of the assumed external load is shown in Figure 2c. As confining pressure increases with depth, all components of the principal stress are assumed to increase proportionally to depth. Initial shear stress τ_0 and normal stress σ_n^0 are then given by

$$\tau_0 = \frac{\sigma_1 - \sigma_3}{2}\sin(2\theta) \tag{1}$$

$$\sigma_n^0 = \frac{\sigma_1 + \sigma_3}{2} - \frac{\sigma_1 - \sigma_3}{2}\cos(2\theta) \tag{2}$$

where θ is the angle of the fault strike with respect to the direction of σ_1.

[8] Total shear and normal stresses (τ^{total} and σ_n^{total}) at each point on the fault are written in the following,

$$\tau^{total}\left(\vec{\xi}, t\right) = \tau_0\left(\vec{\xi}\right) + \Delta\tau\left(\vec{\xi}, t\right) \tag{3}$$

$$\sigma_n^{total}\left(\vec{\xi}, t\right) = \sigma_n^0\left(\vec{\xi}\right) + \Delta\sigma_n\left(\vec{\xi}, t\right) \tag{4}$$

where $\vec{\xi}$ and t are position and time. $\Delta\tau$ and $\Delta\sigma_n$ represent increment stress during dynamic rupture process and are in the form of integral equation, a convolution of Green's function and slip velocity on the fault, calculated based on BIEM [*Aochi et al.*, 2000a]. At the beginning (t = 0), $\Delta\tau$ and $\Delta\sigma_n$ equal to zero, whereas τ_0 and σ_n^0 are given in equations (1) and (2). It should be emphasized that share and normal stresses in equations (3) and (4) are defined with respect to the slip vector on the fault (strike parallel direction). Other four stress components can be calculated in the same way as in *Aochi et al.* [2000a].

[9] For the fault parameters, *Aochi and Fukuyama* [2002] introduced a depth-dependent slip-weakening friction law, shown in Figure 2. When the applied shear stress τ overcomes peak strength σ_p, rupture starts following a slip-weakening relationship between fault function σ and fault slip Δu,

$$\sigma(\Delta u) = \tau_r + \left(\sigma_p - \tau_r\right)\left(1 - \frac{\Delta u}{D_c}\right)H\left(1 - \frac{\Delta u}{D_c}\right). \tag{5}$$

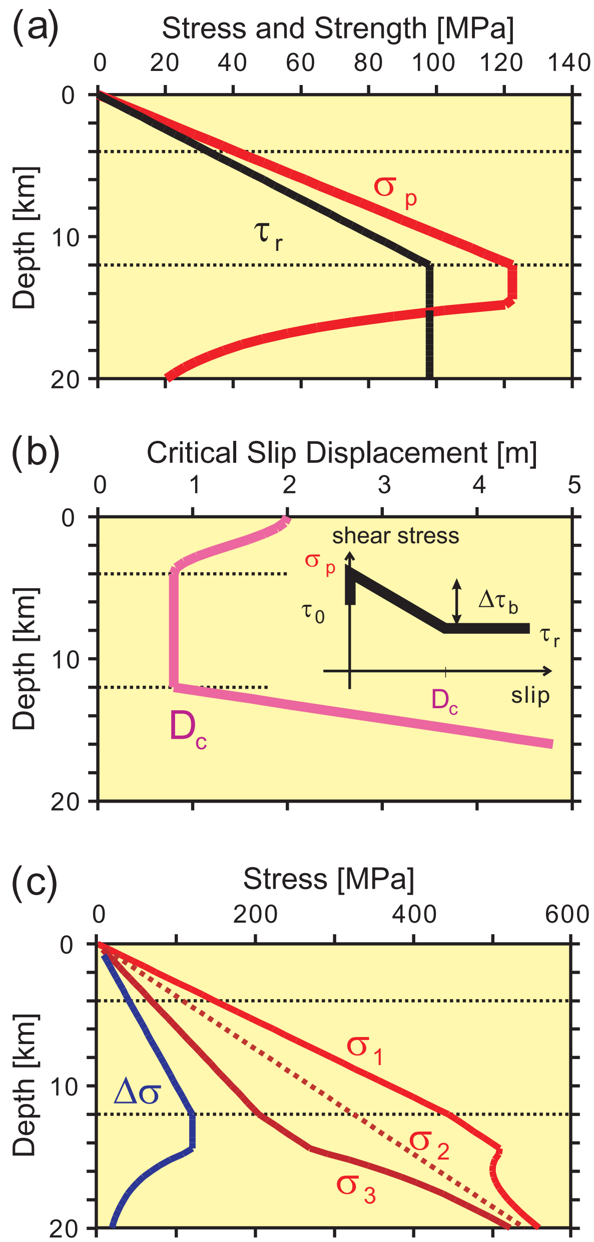

Figure 2. Friction model used by *Aochi and Fukuyama* [2002]. (a) Depth variation of peak strength σ_p and residual stress τ_r. (b) Depth variation of critical slip displacement D_c. A simple slip-weakening law was used. (c) Depth variation of external load (three compressional principal stress $\sigma_1 > \sigma_2 > \sigma_3$) and the deviation $\Delta\tau = (\sigma_1 - \sigma_3)/2$.

Here τ_r is residual strength and D_c is critical slip-weakening distance. Breakdown strength drop $\Delta\tau_b$ is defined by $(\sigma_p - \tau_r)$. $H(\cdot)$ represents the Heaviside function. The slip-weakening friction law was proposed theoretically and numerically [*Ida*, 1972; *Palmer and Rice*, 1973], it was then experimentally observed [*Okubo and Dieterich*, 1984; *Ohnaka et al.*, 1987], modeled theoretically [*Matsu'ura et al.*, 1992], and inferred from seismological modeling of actual earthquake ruptures [*Ide and Takeo*, 1997; *Olsen et al.*, 1997; *Guatteri and Spudich*, 2000]. As clearly seen in the definition of equation (3), this criterion is basically combined with total shear stress τ^{total} in equation (5). In our previous paper [*Aochi and Fukuyama*, 2002] and this study, all parameters, τ_r, σ_p and D_c, are supposed to be temporally invariable, so that it is enough to follow numerically shear stress increment $\Delta\tau$ for practical use. On the other hand, it is possible to introduce a much more complex criterion instead of equation (5). *Aochi et al.* [2002] investigated a dynamic Coulomb law, whose parameters are temporally variable according to normal stress increment $\Delta\sigma_n$. In that case, equation (5) must be combined with both equations (3) and (4) at the same time. However, they reported that increment in normal stress $\Delta\sigma_n$ is generally much smaller than its absolute normal stress level (σ_n^0) when we consider a realistic situation of high confining pressure in the crust, and that, as a result, the frictional parameters do not change drastically with time. That is why, in this paper, we will suppose each frictional parameters are temporally invariable, and consider the effect of their spatial heterogeneity on rupture process.

[10] The product of $\Delta\tau_b$ and D_c determine the fracture energy, a parameter that is the easiest to invert from seismic observations [*Aki*, 1979; *Guatteri and Spudich*, 2000; *Peyrat et al.*, 2002]. The absolute level of stress in the friction law, σ_p and τ_r, are very important because, for an assumed external load (remote tectonic stress), we need the absolute stress field on any segmented, nonplanar fault system. However, the estimation of absolute value of fault parameters is still unsolved. Some seismological analyses proposed that they are much lower than that extrapolated from experimental results [*Bouchon et al.*, 1998; *Spudich et al.*, 1998], as well as other geological observation also suggested low stress along the San Andreas fault. Regardless of the uncertainty, the depth variation of the frictional parameters is often used in the simulation, based on the rheology due to the pressure and temperature with depth, as modeled in *Sibson* [1982], *Scholz* [1988] and *Yamashita and Ohnaka* [1992]. Above the depth of 12 km, the peak strength σ_p as a function of depth z is given by

$$\sigma_p(z) = \sigma_0 + \mu_f \times (P(z) - P_H(z)), \tag{6}$$

where μ_f is frictional coefficient, P and P_H are the confining pressure and hydrostatic pressure, respectively. σ_0 is the cohesive force, but $\sigma_0 = 0$ was assumed in the simulation by *Aochi and Fukuyama* [2002].

[11] *Aochi and Fukuyama* [2002] modeled the rupture process of the Landers earthquake using a numerical boundary integral equation method (BIEM) for nonplanar faults embedded in a 3D unbounded, homogeneous elastic medium [*Aochi et al.*, 2000a]. Time step and square grid size were taken as 0.06 s and 750 m, respectively; and P- and S-wave velocities were 6.20 and 3.52 km/s, respectively. We used mirror sources for approximating the effect of the free surface. A calculation of 400 time steps took about 4×10^5 s of CPU time using 8 to 16 CPUs with fortran90 and MPI on a COMPAQ ES40 Cluster (EV6 500 MHz), although we occasionally ran several jobs for one simulation.

[12] In Animation 1 (available in the HTML version of the article at http://www.g-cubed.org) and Figure A1a, we show a movie of one of the dynamic simulations by *Aochi and Fukuyama* [2002]. We observe that rupture does not propagate on the northern Johnson Valley fault, but chooses the Kickapoo and Homestead Valley faults instead, and then jumps to the northernmost Camp Rock fault. This is the most important feature of the Landers earthquake that they succeeded in reproducing. In the following sections, we will investigate how important were the assumptions they made for rupture propagation, and then discuss

how we may constrain the fault properties from the numerical simulations.

3. Constraint of the Depth-Dependent Friction Law

[13] Although the segmented model of *Aochi and Fukuyama* [2002] reproduced the general features of rupture propagation along the fault system, there are some clear discrepancies between their model and observations. In their simulations, there were several large slip areas along strike in overall agreement with the asperities inferred from kinematic inversion [*Wald and Heaton*, 1994], but the maximum slip was located at a depth of around 12 km. Thus, their model could not produce large slip near the ground surface, although a slip of more than 5 m was observed in the field [*Hart et al.*, 1993]. The discrepancy is due to the depth dependency of friction assumed in the simulation, the depth of 12 km corresponds to the depth where the breakdown strength drop is maximum, as shown in Figure 2. Clearly the assumption of zero peak strength at the ground surface is incorrect. Thus, we have to modify the depth variation of fault properties adapting finite cohesive force σ_0 in equation (6), so that we expect that finite stress could be accumulated and released near the ground surface to produce much fault slip.

[14] As discussed earlier, this is in agreement with many observations of the Landers earthquake. For example, the inversion result by *Bouchon et al.* [1998] showed more than 30 MPa static stress drop at the depth of 4 km. The numerical simulation by *Olsen et al.* [1997] and *Peyrat et al.* [2001] required more than 10 MPa breakdown strength drop at the ground surface as well as in the deeper crust. Figure 3 shows the depth-variation of fault parameters we assumed in the numerical simulation for different cohesive forces. In the deeper part of the fault, we assumed a slip-hardening friction law instead of a slip-weakening law. We assumed a residual stress level τ_r equal to 0 at the surface, and breakdown strength drop $\Delta\tau_b$ to be 20 MPa at the depth of 12 km regardless of the values of σ_0. Friction coefficient $\mu_f = 0.6$ and hydrostatic pressure were assumed.

[15] Let us first compare the dynamic rupture simulations with σ_0 = 0, 5, 10, and 12.5 MPa. Figure 4 shows the final slip distribution on all segments of the Landers earthquake for each value of σ_0. We observe that slip at shallow depth increases as the cohesive force σ_0 increases. Fault slip of more than 5 m was observed on the Homestead Valley and the Camp Rock faults [*Hart et al.*, 1993], so that in order to explain the surface fault slip, breakdown strength drop must be larger than 5 MPa. In our simulations, large slip areas appear near the ground surface, while artificial maximum slips at depth disappear.

[16] In Figure 5, we show synthetic seismograms computed using the discrete wave number method (AXITRA) for the same crustal structure as in *Olsen et al.* [1997] and *Aochi and Fukuyama* [2002]. For each simulation, we show synthetics at station YER which is located in the forward direction of rupture propagation, and where large amplitudes were observed. We observe that the amplitude of the seismogram improves as the cohesive force increases and the fault slip near surface gets larger. We also observe that the width of the pulse becomes narrower as cohesive force increases. This is because cohesion at shallow depths causes large fault slip and fast rupture velocities.

[17] We conclude that a finite cohesive force of more than 5 MPa is required in order to explain the vertical heterogeneity of slip distribution, especially the large slip near surface. Our simulation results indicate the possibility that σ_0 may be as large as 10 MPa, since the synthetic seismograms for this case fits the observed results better than those of the other values of σ_0 (Figure 5). σ_0 = 10 MPa is consistent with the value of 12.5 MPa determined by *Olsen et al.* [1997] and *Peyrat et al.* [2001].

4. Constraints on Horizontal Heterogeneity

4.1. Uniform External Load

[18] Choosing the initial stress field has many degrees of freedom, although the simple assumption in *Aochi and Fukuyama* [2002] was reasonably based on previous geological studies. They found

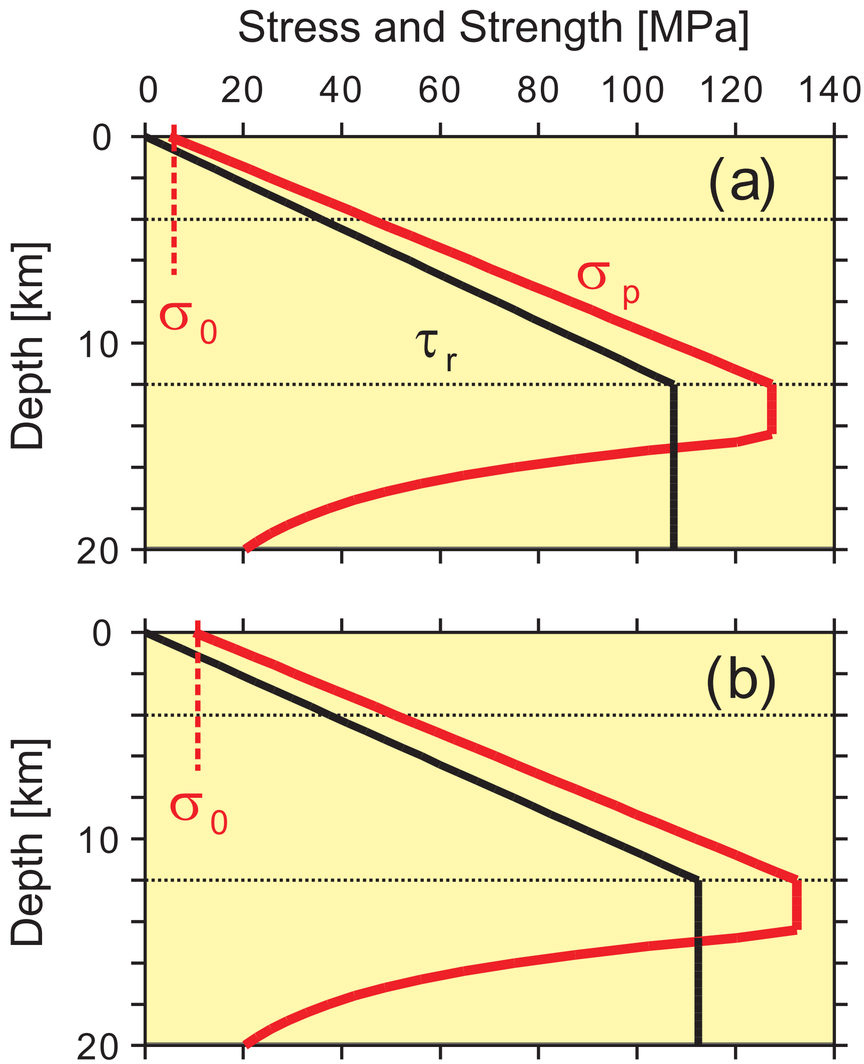

Figure 3. Profile of depth-dependent frictional law with cohesion for surface cohesion (a) σ_0 = 5 MPa, and (b) 10 MPa, respectively.

that a heterogeneous external load (remote tectonic stress) in the southern and northern parts of the model region was essential for the correct fault selection of the Kickapoo and Homestead Valley faults. The selectivity of rupture along a branching fault system is actually very sensitive to the conditions on each branch [*Aochi et al.*, 2000b, 2002].

[19] Before we discuss stress or frictional heterogeneity, let us examine the role of a hypothetical uniform external load on the Landers earthquake propagation. We assume that the direction of maximum uniform principal stress σ_1 is NNW, as shown by the blue arrows in Figure 1 which produces heterogeneous stress field on the fault as shown in Figures 6a and 6b. This principal direction was inferred from the focal mechanisms of the seismicity before and after the 1992 Landers earthquake [*Hauksson*, 1994]. We assumed the same frictional parameters as *Aochi and Fukuyama* [2002], that is, equation (6) with σ_0 = 0. In this uniform external load, we found that the rupture did not jump to the Kickapoo fault, but continued along the Johnson Valley fault as shown in Animation 2 or Figure A1b, causing a completely different history of rupture propagation from the one that was actually observed. We get a maximum fault slip of 5.0 m and a seismic moment of 3.4 × 10^{19} N·m. Thus, under a uniform external load, we have to assume that the Kickapoo and/or Home-

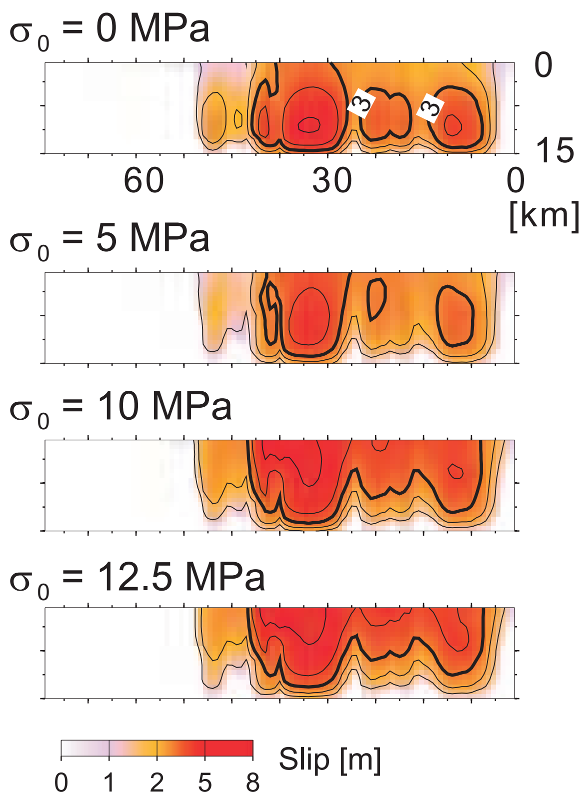

Figure 4. Comparison of final slip distribution for different values of the surface cohesive force σ_0 = 0, 5, 10, and 12.5 MPa. For cohesive forces larger than 5 MPa, large slip areas appear near the surface and artificial zones of large slip at depth disappear.

stead Valley faults are weaker than the northern Johnson Valley fault in order to reproduce the correct rupture path.

4.2. Heterogeneity Produced by a More Complex Friction Law

[20] For the purpose of modeling a weak Kickapoo fault and a strong northern Johnson Valley fault, let us write the frictional parameters σ_p and τ_r in the following way;

$$\sigma_p\left(\vec{\xi}\right) = \mu_s \sigma_n^0\left(\vec{\xi}\right) \tag{7}$$

$$\tau_r\left(\vec{\xi}\right) = \mu_d \sigma_n^0\left(\vec{\xi}\right) \tag{8}$$

where μ_s and μ_d are static and dynamic friction coefficients, and σ_n^0 is the applied normal stress. Hereafter μ_s = 0.6 and hydrostatic pressure are assumed. Now the frictional parameters, σ_p and τ_r, are functions of the fault position $\vec{\xi}$. The initial stress field is shown in Figures 6a and 6b, and possible stress drop in Figure 6c. Normal stress is much lower on the Kickapoo fault than on the northern Johnson Valley fault (Figure 6b), so that it implies a "weak" Kickapoo fault following equation (7). However, the accumulated shear stress (Figure 6a) is also low on the Kickapoo fault, so that it is not possible to produce a positive stress drop on this fault as shown in Figure 6c. Thus rupture can not propagate along the Kickapoo and Homestead Valley faults in this case.

[21] This feature is very interesting. The Kickapoo fault is relatively weak because of a reduced normal stress, but shear stress is not enough to produce slip due to the unfavorable orientation of fault strike with respect to the external load σ_1. This difficulty does not go away even if we introduce the normal stress dependency dynamically into frictional parameters; $\sigma_p(\vec{\xi}, t) = \mu_s\sigma_n(\vec{\xi}, t)$ and $\tau_r(\vec{\xi}, t) = \mu_d\sigma_n(\vec{\xi}, t)$, where the fault parameters are variable with time according to rupture propagation.

[22] Thus we added further heterogeneity of the initial stress field as shown in Figure 7;

$$\sigma_p\left(\vec{\xi}\right) = \mu_s \sigma_n^0\left(\vec{\xi}\right) + \alpha\left(\vec{\xi}\right). \tag{9}$$

Here the space-varying parameter $\alpha(\vec{\xi})$ contains the following information: a strong northern Johnson Valley fault, and weaker and enough loaded Kickapoo, Homestead Valley and Camp Rock faults In this case, we fixed a breakdown strength drop $\Delta\tau_b$ that is a function of normal stress, so that we impose the same heterogeneity $\alpha(\vec{\xi})$ to τ_r;

$$\tau_r\left(\vec{\xi}\right) = \mu_d \sigma_n^0\left(\vec{\xi}\right) + \alpha\left(\vec{\xi}\right). \tag{10}$$

The heterogeneity introduced in equations (9) and (10) is completely different and independent from the one originally included in equations (7) and (8).

[23] Animation 3 shows rupture propagation in this case. Rupture successfully propagates from the Johnson Valley fault to the Camp Rock fault (See also Figure A1d). Besides we observe that rupture transfers through a jog from the Homestead Valley fault to the Emerson fault in contrast to the previous examples without normal stress dependency (Their comparison is shown in Figure A1). There we did not introduce any supplemental

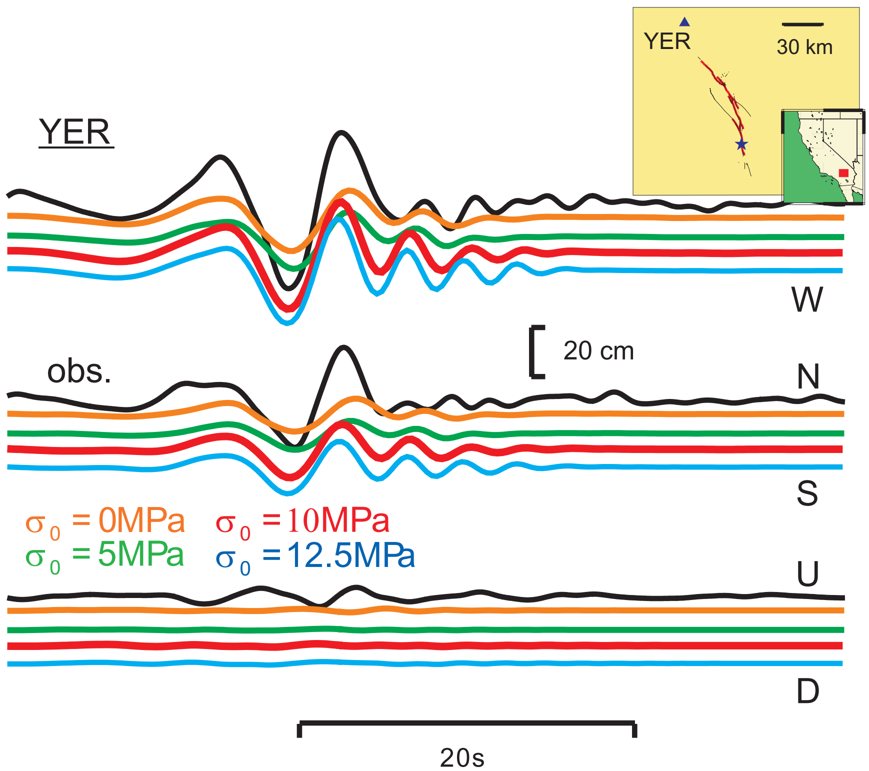

Figure 5. Comparison of synthetic seismogram at the YER station for each simulation shown in Figure 4. As cohesive force increases, the amplitude of synthetic seismograms improves. Seismograms are zero-phrase bandpass filtered between 0.07 and 0.5 Hz.

heterogeneity. As a result, we get a maximum fault slip of 3.67 m and a seismic moment of 5.2×10^{19} N · s.

[24] In conclusion, in order to reproduce the rupture transfer between different fault branches, especially from the Johnson Valley to the Kickapoo and Homestead Valley faults, we needed an additional heterogeneity $\alpha(\vec{\xi})$ which explicitly indicates a weak Kickapoo fault and a strong northern Johnson Valley fault. This seems to be very unlikely. *Rockwell et al.* [2000] investigated paleoseismic data from several trenches and reported that the time intervals from previous event for the southern and northern Johnson Valley and Kickapoo faults were about 5000 years, while those of the Homestead Valley, Emerson and Camp Rock faults were more than 7000 years.

4.3. Stress Heterogeneity Derived From Planar-Fault Simulations

[25] *Olsen et al.* [1997] and *Peyrat et al.* [2001, 2002] successfully determined the heterogeneous initial stress field of the Landers earthquake for a single planar fault through the inversion of the observed ground motion. Since they assumed a single planar fault, the heterogeneity of the stress field can be transferred into the heterogeneity of frictional parameters as long as the amount of available energy to fracture energy is the same in the two models [*Peyrat et al.*, 2002]. That is, a certain relation between τ_0, σ_p and τ_r, that is required stress excess $\Delta\tau_e^{\text{planar}}$ ($\equiv \sigma_p - \tau_0$) and possible stress drop $\Delta\tau^{\text{planar}}$ ($\equiv \tau_0 - \tau_r$) is conserved. In the following, we consider how to map their heterogeneity into our nonplanar fault modeling.

[26] Figure 8 briefly shows the procedure we propose in this section. We start with the uniform external load (remote tectonic stress) as assumed in section 4.1, and indicated by the blue allows in Figure 1. For the purpose of determining the final slip distribution during the earthquake, static stress drop plays a fundamental role. We assume possible stress drop $\Delta\tau$ based on the planar-fault

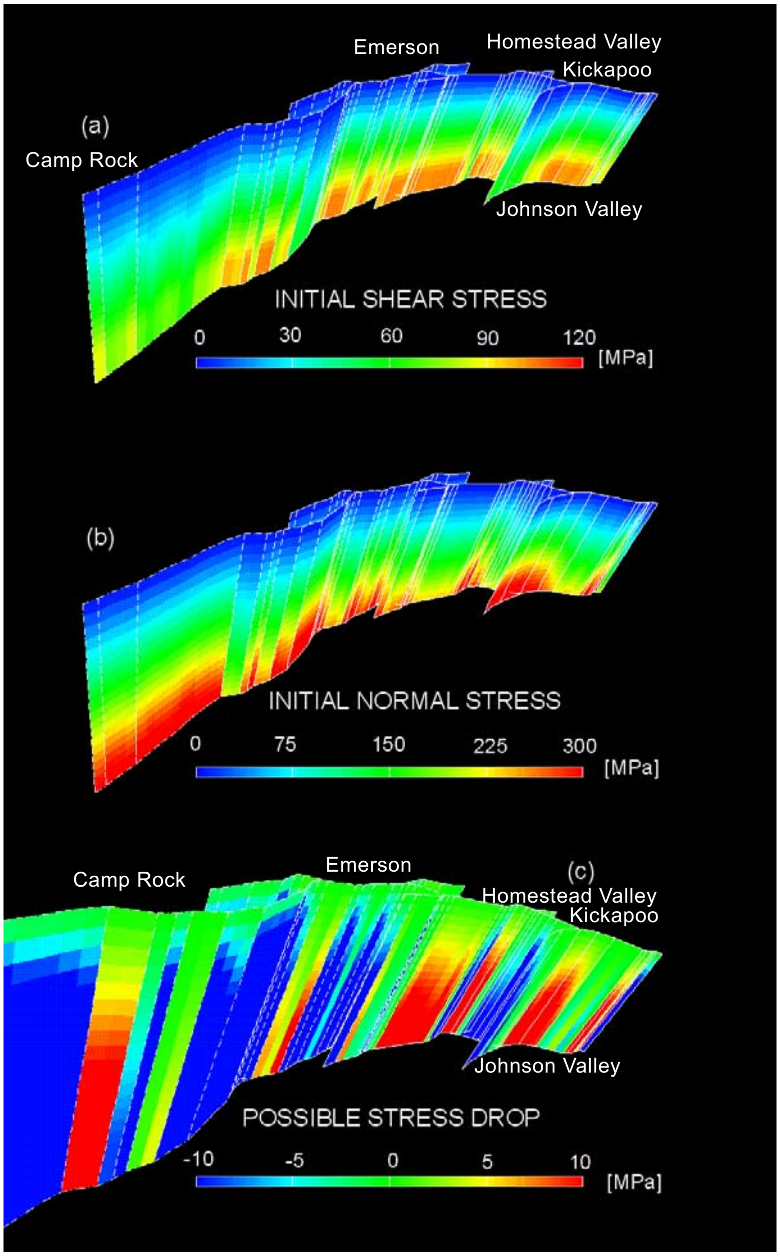

Figure 6. Initial conditions of the model used the Coulomb friction law. (a, b) Initial shear and normal stresses obtained from a uniform external loading system, respectively. (c) Possible stress drop inferred from the above stress field and the Coulomb friction law. On the Kickapoo fault, the applied normal stress is relatively low and peak strength is also low, but the applied initial stress is also low and effective stress drop is very difficult.

inversion of *Peyrat et al.* [2001], as shown in Figure 8 and Figure 9. Thus, we define τ_r by the following expression:

$$\tau_r\left(\vec{\xi}\right) = \tau_0\left(\vec{\xi}\right) - \Delta\tau^{\text{planar}}\left(\vec{\xi}\right) \quad (11)$$

where τ_0 is an assumed uniform external load (remote tectonic stress) and $\Delta\tau^{\text{planar}}$ a heterogeneous stress change inverted from the planar model [*Peyrat et al.*, 2001]. They are functions of fault position $\vec{\xi}$, strike as well as depth. We implicitly prohibit negative friction, so that we set $\tau_r = 0$ in that case.

[27] Although it is possible to use the same peak strength σ_p as in equation (6), we already know

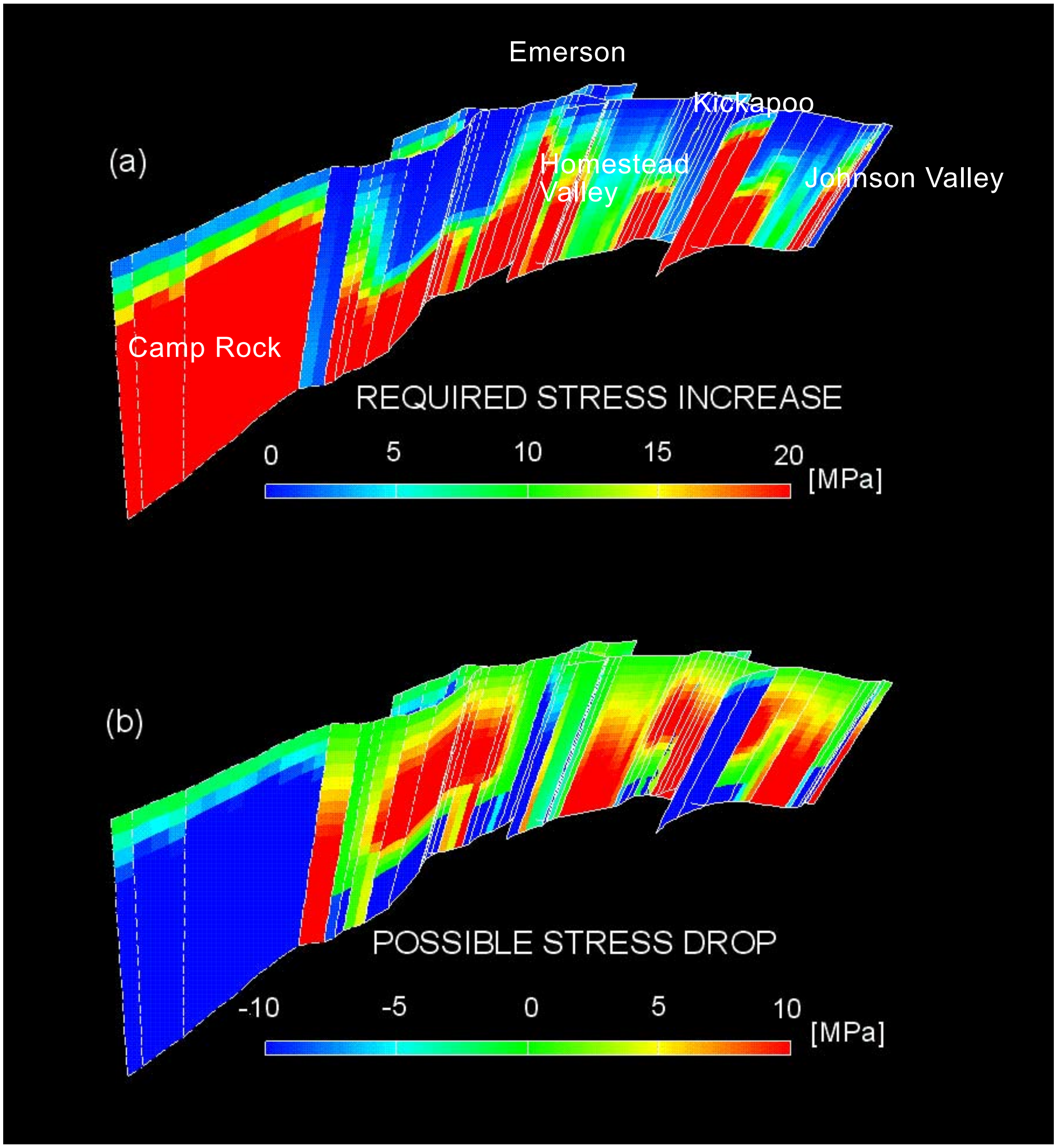

Figure 7. Initial conditions with additional heterogeneity to that in Figure 6. (a) Required stress increase, and (b) possible stress drop. Artificial heterogeneity is given independently from the Coulomb friction law. In this case, the Kickapoo fault is weak enough compared to the applied initial shear stress.

that this did not work in the case of the uniform external load. Thus, in order for rupture to progress correctly, we also have to change peak strength σ_p – or strictly speaking, the stress increase ($\Delta\tau_e$) from the assumed initial stress field ($\sigma_p - \tau_0$). Actually, we not only give the stress increase $\Delta\tau_e^{planar}$ of the planar fault simulation [*Peyrat et al.*, 2001], but also a small additional heterogeneity $\beta(\vec{\xi})$.

$$\sigma_p\left(\vec{\xi}\right) = \tau_0\left(\vec{\xi}\right) + \Delta\tau_e^{\text{planar}}\left(\vec{\xi}\right) + \beta\left(\vec{\xi}\right) \tag{12}$$

That is necessary because, without a small $\beta(\vec{\xi})$, the rupture does not propagate. In the simulations the

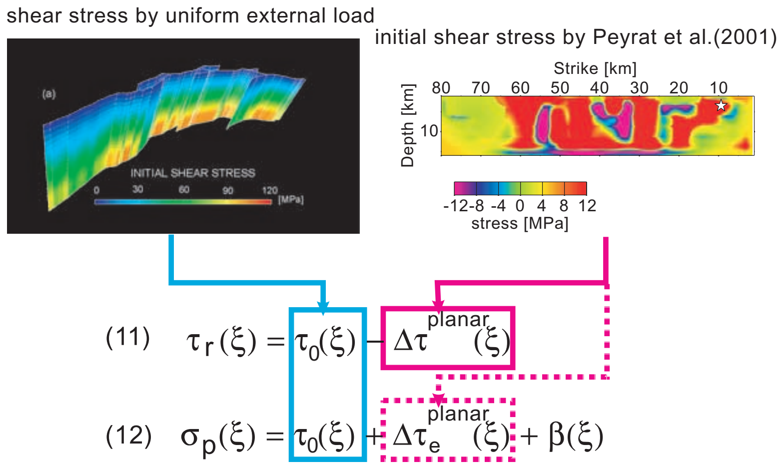

Figure 8. Procedure for mapping stress heterogeneity determined from a planar fault model into a segemented, nonplanar fault. A uniform external load (remote stress) imposes a heterogeneous initial shear stress τ_0 on the fault as shown in the left panel on the top (see also Figure 9a). First we constrain the residual stress τ_r by the stress drop $\Delta\tau^{planar}$ (see Figure 9b) based on the initial condition of *Peyrat et al.* [2001] (right panel on the top), as shown in equation (5). In a second step, we adjust the peak strength σ_p by the required stress excess $\Delta\tau_e^{planar}$ of the planar fault simulation, as shown in equation (6). Here $\Delta\tau_e^{planar} = 12.5 - \Delta\tau^{planar}$. We further need further heterogeneity β which indicates a week Kickapoo fault and a strong northern Johnson Valley fault (See Figure 9c).

rupture never reached the branching point of the Kickapoo fault, because the nonplanarity of the fault perturbs the stress field and actually reduces shear stress with respect to the planar case. Thus we had to increase the available potential strain energy release by increasing $\beta(\vec{\xi})$. An even more critical problem in nonplanar fault modeling is that we need to introduce additional information so that rupture chooses the Kickapoo fault when it reaches the branching point. As shown in the previous section 4.1, when the frictional parameters (σ_p and τ_r) are the same on both subfaults, rupture clearly prefers the northern Johnson Valley fault. Thus, in order to obtain the correct fault selection, a weak Kickapoo fault is necessary. As a result, we assume, in the expression of $\beta(\vec{\xi})$, that the northern Johnson Valley fault is strong, and that the Kickapoo, southern Homestead Valley and Camp Rock faults are weak. Now we find that frictional parameters σ_p and τ_r are different from equations (7) and (8). Furthermore, since we give derivative additional stress $\Delta\tau^{planar}$ and $\Delta\tau_e^{planar}$ in equations (11) and (12), regional stress given by external load is hidden behind the heterogeneity inverted from the planar fault simulation. Thus we can actually use an almost arbitrary initial stress τ_0, otherwise it is also possible to begin with σ_p given by equation (7) depending on applied normal stress, and constrain the other parameters τ_0 and τ_r with the deviations $\Delta\tau^{planar}$ and $\Delta\tau_e^{planar}$.

[28] Animation 4 (see also Figure A1d) shows rupture propagation for this model. Rupture successfully propagates along the Kickapoo and Homestead Valley faults, then it transfers to the last segment, the Emerson and Camp Rock faults, and finally it is gradually arrested. The process of rupture propagation is very similar to that of *Wald and Heaton* [1994] and *Peyrat et al.* [2001]. However, even though the stress drop $\Delta\tau^{planar}$ is the same as theirs, the amount of final slip in our simulation is smaller due to the perturbation of the stress field by the geometry of the fault system. The maximum fault slip is 3.6 m, while theirs reached 6 m. We got a seismic moment of 5.3×10^{19} N·m, which is somewhat less than the 7.0×10^{19} N·m obtained in the planar simulation [*Peyrat et al.*, 2001].

[29] In Figure 10, we compare synthetic seismograms obtained from our simulation with the

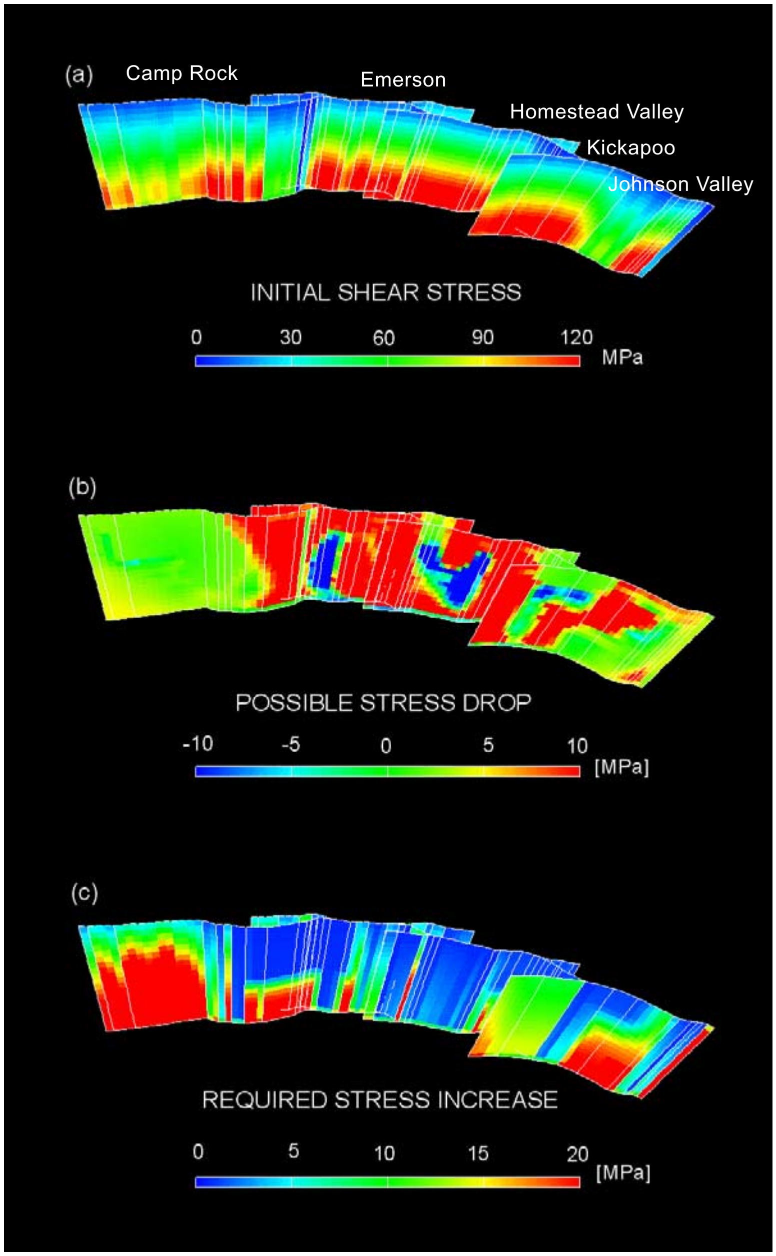

Figure 9. Initial stress distribution constrained by the mapping of the planar fault simulation [*Peyrat et al.*, 2001]. (a) Initial shear stress produced by the uniform external loading system. (b) Possible stress drop, the difference between the initial shear stress and the residual stress drop ($\tau_0 - \tau_r$), mapped from the planar-fault simulation. (c) Required stress increase, the difference between the peak strength and the initial shear stress ($\sigma_p - \tau_0$), obtained after adding artificial heterogeneity.

observed ground displacement records and those produced by the previous model of Animation 1 or Figure A1d [*Aochi and Fukuyama*, 2002]. We show recordings at the YER, SVD, and PFO stations which are located in different directions from the fault. At YER, located in the forward direction of rupture propagation, the amplitude of the synthetics does not fit the observation well, because, as we explained above, fault slip is still underestimated in our model. Ground motion at

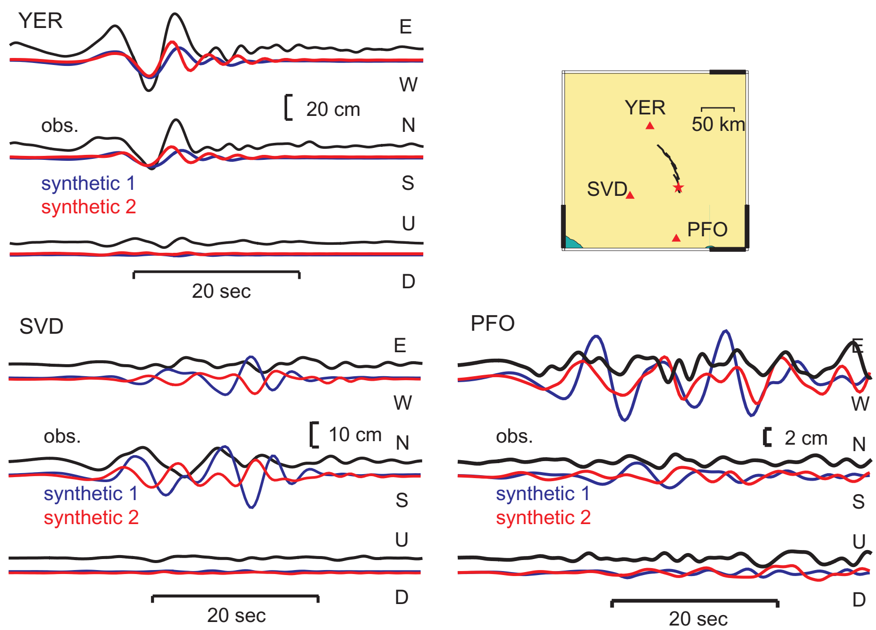

Figure 10. Synthetic seismograms at YER, SVD, and PFO stations (synthetic 2). At SVD and PFO stations, synthetic waveforms becomes much closer to the observed ones because the slip distribution is much closer to that constrained by planar-fault simulation. As a reference, we also show synthetic seismograms obtained from the uniform stress model of Animation 1 (synthetic 1). Seismograms are zero-phase bandpass filtered between 0.07 and 0.5 Hz.

YER is affected by directivity much more than by the details of rupture propagation. On the other hand, at SVD and PFO where rupture directivity is small, we observe that the synthetics have improved from the previous simulation [*Aochi and Fukuyama*, 2002] and become similar to the observed records. That is because we constrained stress drop ($\tau_0 - \tau_r$) so that the final slip distribution has significantly improved (see also Figures A1a and A1d).

5. Summary

[30] In this paper, we tried to determine frictional parameters for the dynamic rupture simulation of the 1992 Landers earthquake along a nonplanar fault system. We found that a finite cohesive force σ_0 (order of 10 MPa) is required in order to reproduce large slip areas near the surface. Otherwise, stress is never accumulated or released around the surface, so that it inhibits large slip near the surface which is sharp contrast with geological and geodetic observations.

[31] Modeling heterogeneity along fault strikes is much more difficult. We found that the heterogeneity produced by simple variations of normal stress derived from simple tectonic stress models could not explain the observations without an additional heterogeneity of internal origin. Then we observed that the stress heterogeneity inferred by the planar fault inversions [*Peyrat et al.*, 2001] improved the details of the rupture process and the fit to the seismograms observed around the fault system. In every case, we needed to adjust frictional parameters such as a weak Kickapoo fault and a strong northern Johnson Valley fault in order to obtain the correct selection of rupture propagation. We remark that the improvement obtained by the planar fault modeling is independent of the mathematical expressions, equations (6), (7), and (8), assumed in the other part of this study. Actually, we do not need much information about absolute stress, equations (1) and (2), since we use only the deviation of stress. It is clear that the state of regional stress is hidden by the heterogeneity inverted from the planar fault models. It will be a key point whether or not we

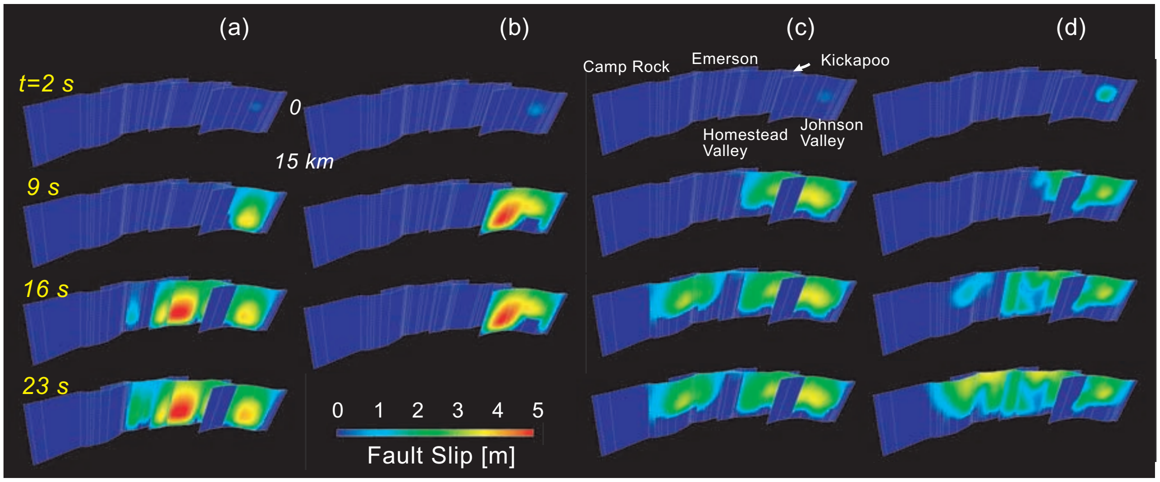

Figure A1. Snapshots of each simulation shown in this study. (a) The previous simulations of *Aochi and Fukuyama* [2002]. Its movie is in Animation 1. (b) The case of uniform loading stress (Animation 2). Rupture propagates on the Johnson Valley fault. (c) The model including applied normal stress in frictional parameters (Animation 3). (d) The model with initial condition similar to that of the planar fault simulation (Animation 4).

can find this kind of information for realistic rupture models.

Appendix: Snapshots of Dynamic Simulation

[32] Simulation results are given as movie files in this manuscript. In Figure A1, we further show their snapshots in static images for convenience.

Acknowledgments

[33] We would like to thank Ruth Harris, an anonymous reviewer and Rick O'Connell whose comments help us to improve this manuscript. For numerical simulations, we used the parallel computer at the Département de Simulation Physique et Numérique de l'Institut de Physique du Globe de Paris (IPGP). This research was supported by the profect "Rupture et changement d'échelle" of ACI Catastrophes Naturelles of the Ministère de la Recherche, France.

References

Aki, K., Characterization of barriers of an earthquake fault, *J. Geophys. Res.*, *84*, 6140–6148, 1979.

Aochi, H., and E. Fukuyama, Three-dimensional nonplanar simulation of the 1992 Landers earthquake, *J. Geophys. Res.*, *107*(B2), 2035, doi:10.1029/2000JB000061, 2002.

Aochi, H., E. Fukuyama, and M. Matsu'ura, Spontaneous Rupture Propagation on a Non-planar Fault in 3-D Elastic Medium, *PAGEOPH*, *157*, 2003–2027, 2000a.

Aochi, H., E. Fukuyama, and M. Matsu'ura, Selectivity of spontaneous rupture propagation on a branched fault, *Geophys. Res. Lett.*, *27*, 3635–3638, 2000b.

Aochi, H., R. Madariaga, and E. Fukuyama, Effect of normal stress during rupture propagation along nonplanar faults, *J. Geophys. Res.*, *107*(B2), 2038, doi:10.1029/2001JB000500, 2002.

Boatwright, J., and M. Cocco, Frictional constraints on crustal faulting, *J. Geophys. Res.*, *101*, 13,895–13,909, 1996.

Bouchon, M., M. Campillo, and F. Cotton, Stress field associated with the rupture of the 1992 Landers, California, earthquake and its implications concerning the fault strength at the onset of the earthquake, *J. Geophys. Res.*, *103*, 21,091–21,097, 1998a.

Bouchon, M., H. Sekiguchi, K. Irikura, and T. Iwata, Some characteristics of the stress field of the 1995 Hyogo-ken Nanbu (Kobe) earthquake, *J. Geophys. Res.*, *103*, 24,271–24,282, 1998b.

Cochard, A., and R. Madariaga, Dynamic faulting under rate-dependent friction, *PAGEOPH*, *142*, 419–445, 1994.

Day, S., G. Yu, and D. J. Wald, Dynamic stress changes during earthquake rupture, *Bull. Seismol. Soc. Am.*, *88*, 512–522, 1998.

Dokka, R. K., and C. J. Travis, Role of the eastern California shear zone in accommodating Pacific-North American plate motion, *Geophys. Res. Lett.*, *17*, 1323–1326, 1990.

Fukuyama, E., and R. Madariaga, Integral equation method for plane crack with arbitrary shape in 3d elastic medium, *Bull. Seismol. Soc. Am.*, *85*, 614–628, 1995.

Guatteri, M., and P. Spudich, What can strong-motion data tell us about slip-weakening fault-friction laws?, *Bull. Seismol. Soc. Am.*, *90*, 98–116, 2000.

Guatteri, M., G. Beroza, and P. Spudich, Inferring rate and state friction parameters from a rupture model of the 1995 Hyogo-ken Nanbu (Kobe) Japan earthquake, *J. Geophys. Res.*, *106*, 26,511–26,522, 2001.

Harris, R. A., and S. M. Day, Dynamics of fault interaction: Parallel strike-slip faults, *Geophys. Res. Lett.*, *98*, 4461–4472, 1993.

Harris, R. A., and S. M. Day, Dynamic 3D simulations of earthquakes on en echelon faults, *Geophys. Res. Lett.*, *26*, 2089–2092, 1999.

Harris, R. A., R. J. Archuleta, and S. M. Day, Fault step and the dynamic rupture process: 2-D numerical simulations of a spontaneously propagating shear fracture, *Geophys. Res. Lett.*, *18*, 893–896, 1991.

Hart, E. W., W. A. Bryant, and J. A. Treiman, Surface faulting associated with the June 1992 Landers earthquake, California, *Calif. Geol.*, *46*, 10–16, 1993.

Hauksson, E., State of stress from focal mechanisms before and after the 1992 Landers earthquake sequence, *Bull. Seismol. Soc. Am.*, *84*, 917–934, 1994.

Ida, Y., Cohesive force across the tip of a longitudinal-shear crack and Griffith's specific surface energy, *J. Geophys. Res.*, *77*, 3796–3805, 1972.

Ide, S., and M. Takeo, Determination of constitutive relations of fault slip based on seismic wave analysis, *J. Geophys. Res.*, *102*, 27,379–27,391, 1997.

Kame, N., and T. Yamashita, Dynamic nucleation process of shallow earthquake faulting in a fault zone, *Geophys. J. Int.*, *128*, 204–216, 1997.

Kame, N., and T. Yamashita, Simulation of the spontaneous growth of a dynamic crack without constraints on the crack tip path, *Geophys. J. Int.*, *139*, 345–358, 1999.

Kase, Y., and K. Kuge, Numerical simulation of spontaneous rupture processes on two non-coplanar faults: The effect of geometry on fault interaction, *Geophys. J. Int.*, *135*, 911–922, 1998.

Kase, Y., and K. Kuge, Rupture propagation beyond fault discontinuities: Significance of fault strike and location, *Geophys. J. Int.*, *147*, 330–342, 2001.

Koller, M. G., M. Bonnet, and R. Madariaga, Modeling of dynamical crack propagation using time-domain boundary integral equations, *Wave Motion*, *16*, 339–366, 1992.

Madariaga, R., On the relation between seismic moment and stress drop in the presence of stress and strength heterogeneity, *J. Geophys. Res.*, *84*, 2243–2250, 1979.

Matsu'ura, M., H. Kataoka, and B. Shibazaki, Slip-dependent friction law and nucleation processes in earthquake rupture, *Tectonophysics*, *211*, 135–148, 1992.

Okubo, P. G., and J. H. Dieterich, Effects of physical fault properties on frictional instabilities produced on simulated faults, *J. Geophys. Res.*, *89*, 5817–5827, 1984.

Ohnaka, M., Y. Kuwahara, and K. Yamamoto, Constitutive relations between dynamic physical parameters near a tip of the propagating slip zone during stick-slip shear failure, *Tectonophys.*, *144*, 109–125, 1987.

Olsen, K. B., R. Madariaga, and R. J. Archuleta, Three-Dimensional dynamic simulation of the 1992 Landers Earthquake, *Science*, *278*, 834–838, 1997.

Palmer, A. C., and J. R. Rice, The growth of slip surfaces in the progressive failure of over-consolidated clay, *Proc. R. Soc. London Ser. A*, *332*, 527–548, 1973.

Peyrat, S., K. B. Olsen, and R. Madariaga, Dynamic modeling of the 1992 Landers Earthquake, *J. Geophys. Res.*, *106*, 26,467–26,482, 2001.

Peyrat, S., K. B. Olsen, and R. Madariaga, La dynamique des tremblements de terre vue à travers le séisme de Landers du 28 Juin 1992, *C. R. Acad. Sci. Paris*, *330*, 235–248, 2002.

Rockwell, T. K., S. Lindvall, M. Herzberg, D. Murbach, T. Dawson, and G. Berger, Paleoseismology of the Johnson Valley, Kickapoo, and Homestead Valley Faults: Clustering of earthquakes in the eastern California shear zone, *Bull. Seismol. Soc. Am.*, *90*, 1200–1236, 2000.

Scholz, C. H., The brittle-plastic transition and the depth of seismic faulting, *Geol. Rund.*, *77*, 319–328, 1988.

Sibson, R. H., Fault zone models, heat flow, and the depth distribution of earthquakes in the continental crust of the United States, *Bull. Seismol. Soc. Am.*, *72*, 151–163, 1982.

Sowers, J. M., J. R. Unruh, W. R. Lettis, and T. D. Rubin, Relationship of the Kickapoo Fault to the Johnson Valley and Homestead Valley Faults, San Bernardino Country, California, *Bull. Seismol. Soc. Am.*, *84*, 528–536, 1994.

Spudich, P., M. Guatteri, K. Otsuki, and J. Minagawa, Use of Fault Striations and Dislocation Models to Infer Tectonic Shear Stress during the 1995 Hyogo-ken Nanbu (Kobe) Earthquake, *J. Geophys. Res.*, *88*, 413–427, 1998.

Tada, T., and T. Yamashita, Non-hypersingular boundary integral equations for two-dimensional non-planar crack analysis, *Geophys. J. Int.*, *130*, 269–282, 1997.

Unruh, J. R., W. R. Lettis, and J. M. Sowers, Kinematic Interpretation of the 1992 Landers Earthquake, *Bull. Seismol. Soc. Am.*, *84*, 537–546, 1994.

Wald, D. J., and T. H. Heaton, Spatial and temporal distribution of slip for the 1992 Landers, California, earthquake, *Bull. Seismol. Soc. Am.*, *84*, 668–691, 1994.

Yamashita, T., and M. Ohnaka, Precursory surface deformation expected from a strike-slip fault model into which rheological properties of the lithosphere are incorporated, *Tectonophysics*, *211*, 179–199, 1992.